

Single particle in a reflection-asymmetric potential

Y. Y. Wang¹ and Z. X. Ren^{2,*}

¹*School of Physics and Nuclear Energy Engineering and International Research Center for Nuclei and Particles in the Cosmos, Beihang University, Beijing 100191, China*

²*State Key Laboratory of Nuclear Physics and Technology, School of Physics, Peking University, Beijing 100871, China*

(Dated: October 13, 2018)

Single particle moving in a reflection-asymmetric potential is investigated by solving the Schrödinger equation of the reflection-asymmetric Nilsson Hamiltonian with the imaginary time method in 3D lattice space and the harmonic oscillator basis expansion method. In the 3D lattice calculation, the l^2 divergence problem is discussed and is avoided by introducing a damping function; the $\langle l^2 \rangle_N$ term in non-spherical case is calculated by an equivalent N -independent operator form; and the harmonic oscillator potential is modified to improve the convergence of the iteration. The efficiency of these numerical techniques is demonstrated by solving the spherical Nilsson Hamiltonian in 3D lattice space. The evolution of the single-particle levels in a reflection-asymmetric deformed potential is obtained and discussed by the above two numerical methods, and their consistency is shown in the obtained single-particle energy with difference smaller than $10^{-4} [\hbar\omega_0]$.

PACS numbers: 21.10.Re, 21.60.Ev, 27.70.+q, 21.60.Jz

I. INTRODUCTION

Nuclear shape provides an intuitive understanding of spatial density distributions of atomic nuclei [1, 2], and manifests itself in various exotic nuclear phenomena, such as halo phenomena in spherical [3–5] and deformed nuclei [6–8], superdeformation rotational band [9], tidal waves [10, 11], chiral rotation [12–14], wobbling motion [1, 15] and nuclear fissions [1, 2].

The nuclei were assumed to be spherical shape in the early history of nuclear physics [16]. Based on the observation of large quadrupole moments in some nuclei, Rainwater pointed out that those nuclei might have deformed shapes [17]. Then Bohr and Mottelson proposed the nuclear collective model, which successfully explained the observation of rotational band structures [18]. In a more microscopical way, Nilsson extended the spherical shell model to deformed case by introducing the quadrupole deformation degree of freedom [19]. Since its introduction, the Nilsson model has achieved great success in accounting for most of the observed features of single-particle levels in deformed nuclei, and provides a proper microscopic basis to understand the nuclear structural properties.

With the first observation of negative-parity states in the even-even radium region by Berkeley group in 1950s [20], the possibility arose that nuclei might have a reflection-asymmetric shape [21, 22]. In order to investigate those nuclei, one can calculate the single-particle energies in an average potential with reflection-asymmetric degree of freedom. Dutt and Mukherjee developed the reflection-asymmetric Nilsson model and investigated the single-particle motion in such a given potential [23], and

based on this Hamiltonian many investigations have been performed [24–27]. The density functional theory (DFT) provides an average potential in a self-consistent way and has achieved great success in describing not only the single-particle motions [28–32] but also the nuclear collective excitation modes [33–43]. A series of works on the reflection-asymmetric shaped nuclei have been done based on various DFTs [44–51]. Even if the DFTs are based on the various effective nucleon-nucleon interactions, the problem to be solved is the single-particle motion in a mean-field potential with possible deformation.

In order to solve the single-particle motion in a mean-field potential, the harmonic oscillator (H.O.) basis expansion method has been widely used and achieved great success [31, 32, 39]. However, for nuclear phenomena with large spatial distribution, such as halo phenomena or nuclear fissions [6], a large basis space is needed to get a convergence result. In a more efficient way, one can solve the equation of the motion in coordinate space.

The imaginary time method (ITM) [52, 53] is a powerful approach for solving equations of motion in coordinate spaces, and it has been successfully applied to solve the Schrödinger equation and Dirac equation in 3D lattice space [53–56].

In this paper, the ITM is used to solve the Schrödinger equation of the reflection-asymmetric Nilsson Hamiltonian in 3D lattice space, and the results obtained by the H.O. basis expansion method are compared with those from 3D lattice calculation.

The paper is organized as follows, the reflection-asymmetric Nilsson Hamiltonian, together with the H.O. basis expansion method and the ITM in 3D lattice space will be briefly introduced in Sec. II. In Sec. III, the parameters for the reflection-asymmetric Nilsson Hamiltonian, and the numerical details for the H.O. basis method and 3D lattice calculation are presented. The discussions and treatments of the challenges, including the l^2 diver-

*Electronic address: zhxr1992@pku.edu.cn

gence problem, the calculation of $\langle \mathbf{l}^2 \rangle_N$ term, the convergence problem of the iteration for solving Nilsson Hamiltonian in 3D lattice space, and the efficiency of these treatments are given in Sec. IV. Section V is devoted to the single-particle motion in a reflection-asymmetric potential. Summary and perspectives are given in Sec. VI.

II. THEORETICAL FRAMEWORK

A. Reflection-asymmetric Nilsson Hamiltonian

In present work, the single-particle motion in a reflection-asymmetric potential is investigated by calculating the eigen energies and eigen wave functions of a reflection-asymmetric Nilsson Hamiltonian [23],

$$\hat{h} = -\frac{\hbar^2}{2m}\Delta + V(r, \theta) + Cl \cdot \mathbf{s} + D[\mathbf{l}^2 - \langle \mathbf{l}^2 \rangle_N], \quad (1)$$

with $-\hbar^2\Delta/2m$ the kinetic energy, $V(r, \theta)$ the reflection-asymmetric deformed potential, $Cl \cdot \mathbf{s}$ the spin-orbit term and the $D[\mathbf{l}^2 - \langle \mathbf{l}^2 \rangle_N]$ term.

The reflection-asymmetric deformed potential $V(r, \theta)$ has the form

$$V(r, \theta) = \frac{1}{2}m\omega_0^2 r^2 \left[1 + a_1 Y_{10}(\theta, \phi) + a_2 Y_{20}(\theta, \phi) + a_3 Y_{30}(\theta, \phi) \right], \quad (2)$$

with parameters a_1 , a_2 and a_3 describing the dipole, quadrupole and octupole deformation, respectively. Assuming that the nuclear density is constant and distributes within an equipotential surface, one can determine the relations among the parameters a_1 , a_2 and a_3 by restricting the center of mass of nuclei coincided with the origin of the coordinate system and the volume conservation,

$$a_1 \sim \frac{9\sqrt{3}}{2\sqrt{35}\pi} a_2 a_3, \quad \omega_0^2 \sim \left[1 + \frac{5}{16\pi} (a_2^2 + a_3^2) \right] \hat{\omega}_0, \quad (3)$$

where the higher order terms of a_1, a_2 and a_3 are neglected, and $\hat{\omega}_0$ corresponds to the frequency of the potential in spherical case. The parameters a_2 and a_3 can be related with the commonly used quadrupole and octupole deformation parameters β_2 and β_3 ,

$$a_2 = -2\beta_2, \quad a_3 = -2\beta_3. \quad (4)$$

The spin orbit term $Cl \cdot \mathbf{s}$ is essential to reproduce the right magic number [16]. The $D[\mathbf{l}^2 - \langle \mathbf{l}^2 \rangle_N]$ term, in which $\langle \mathbf{l}^2 \rangle_N = N(N+3)/2$ is the expectation value of \mathbf{l}^2 averaged over one spherical major shell with quantum number N , has the effect of interpolating between the oscillator and the square well and thus reproducing effectively the Woods-Saxon radial shape [57]. In general, the constants C and D are given in the form of the Nilsson parameters κ and μ ,

$$C = -2\hbar\hat{\omega}_0\kappa, \quad D = -\hbar\hat{\omega}_0\mu. \quad (5)$$

The values of κ and μ depend on the mass number of investigated nuclei, and one choice is [58],

$$\left. \begin{aligned} \kappa_p &= 0.0766 - 0.0779 \frac{A}{1000} \\ \mu_p &= 0.493 + 0.649 \frac{A}{1000} \end{aligned} \right\} \text{for proton and,} \quad (6)$$

$$\left. \begin{aligned} \kappa_n &= 0.0641 - 0.0026 \frac{A}{1000} \\ \mu_n &= 0.624 - 1.234 \frac{A}{1000} \end{aligned} \right\} \text{for neutron.} \quad (7)$$

B. The numerical methods

In present work, two numerical methods are employed to obtain the eigen energies of the reflection-asymmetric Nilsson Hamiltonian. One can diagonalize the Hamiltonian (1) in spherical harmonic oscillator basis $|Nlj\Omega\rangle$, the corresponding quantum numbers are denoted by N , l , j and Ω , i.e., the total number of the oscillator quanta, the orbit angular momentum, the total angular momentum and its component along z -axis.

The ITM is an iterative method for solving the equation of the motion with arbitrary shape. The basic ideal of ITM is to replace time with an imaginary one, and the evolution of the wave function reads [52],

$$e^{-i\hat{h}t}|\psi_0\rangle \xrightarrow{t \rightarrow -i\tau} e^{-\hat{h}\tau}|\psi_0\rangle, \quad (8)$$

where $|\psi_0\rangle$ is an initial wave function and \hat{h} is the Hamiltonian.

With the eigenstates $\{\phi_k\}$ of the Hamiltonian \hat{h} corresponding to the eigenvalues $\{\varepsilon_k\}$, the evolution of the wave function $|\psi(\tau)\rangle = e^{-\hat{h}\tau}|\psi_0\rangle$ can be written as

$$|\psi(\tau)\rangle = e^{-\hat{h}\tau}|\psi_0\rangle = \sum_k e^{-\varepsilon_k\tau} |\phi_k\rangle \langle \phi_k | \psi_0 \rangle, \quad (9)$$

where $\varepsilon_1 \leq \varepsilon_2 \leq \dots$. For $\tau \rightarrow \infty$, $|\psi(\tau)\rangle$ will approach the ground state wave function of \hat{h} so long as $\langle \phi_1 | \psi_0 \rangle \neq 0$.

In practice, the imaginary time τ is discrete with the interval $\Delta\tau$, i.e., $\tau = N\Delta\tau$. The wave function at $\tau = (n+1)\Delta\tau$ is obtained from the wave function at $\tau = n\Delta\tau$ by expanding the exponential evolution operator $e^{-\Delta\tau\hat{h}}$ to the linear order of $\Delta\tau$,

$$|\psi^{(n+1)}\rangle = (1 - \Delta\tau\hat{h})|\psi^{(n)}\rangle. \quad (10)$$

Since this evolution is not unitary, the wave function should be normalized at every step.

However, convergence feature of Eq. (10) is not so satisfactory as discussed in detail in Ref. [59]. The essential reason for this problem is that all energy components are propagated with the same step size $\Delta\tau$ and thus the actual evolution of each components is proportional to its

energy, which can be seen by expanding $|\psi^{(n)}\rangle$ in Eq. (10) with the eigenstates $\{\phi_k\}$,

$$|\psi^{(n+1)}\rangle = (1 - \Delta\tau\hat{h})|\psi^{(n)}\rangle = \sum_k (1 - \Delta\tau\varepsilon_k)|\phi_k\rangle\langle\phi_k|\psi^{(n)}\rangle. \quad (11)$$

Considering that the high energy components are usually dominated by the kinetic energy, a simple iteration scheme Eq.(10) is improved by kinetic-energy damping [59, 60],

$$|\psi^{(n+1)}\rangle = \left\{ 1 - \frac{\delta}{\hat{T} + E_0} (\hat{h} - \langle\psi^{(n)}|\hat{h}|\psi^{(n)}\rangle) \right\} |\psi^{(n)}\rangle, \quad (12)$$

where $\hat{T} = (\hbar^2/2m)\hat{\mathbf{p}}^2$ is the operator of kinetic energy, δ and E_0 are numerical parameters. To get a stable and fast convergence, E_0 should be chosen typically of the order of the depth of the potential, and δ is of order of 0.1, \dots , 0.8. Although larger δ can yield faster convergence, the evolution more easily meets the pathological conditions.

To find excited states, one can start with a set of initial wave functions and orthonormalize them during the evolution by the Gram-Schmidt method. This method has been successfully employed in the 3D coordinate-space calculations for nonrelativistic systems [54].

III. NUMERICAL DETAILS

In the present work, the Nilsson parameters adopted are $\kappa = 0.0589167$ and $\mu = 0.640323$, which correspond to the proton potential with mass number $A = 227$. For simplicity, in the following calculations the natural units $\hbar = \omega_0 = m = 1$ are used.

For the H.O. basis calculation, the $N_{\text{shell}} = 20$ of the spherical oscillator is chosen in the diagonalization procedure. By increasing N_{shell} from 20 to 24 in the $(\beta_2, \beta_3) = (0.3, 0.1)$ case, the changes of the obtained single particle energies below 7 $[\hbar\omega_0]$ are small than 10^{-5} $[\hbar\omega_0]$, suggesting that $N_{\text{shell}} = 20$ is accurate enough.

For the 3D lattice calculation, the step size $d = 0.6$ $[\sqrt{\hbar/m\omega_0}]$ and grid number $n = 30$ are chosen along x , y and z directions. The distribution of the grids in each direction is symmetric respect to the origin of the coordinate system, and the spatial derivatives are performed in momentum space with the fast Fourier transform [54, 56].

IV. CHALLENGES IN THE 3D LATTICE CALCULATION

When solving the Nilsson Hamiltonian (1) in 3D lattice space by ITM, one will meet several challenges, including the l^2 divergence problem, the calculation of the $\langle l^2 \rangle_N$ term, and the convergence of the iteration due to the

harmonic oscillator potential. The discussions and treatments of these challenges will be given in the following. By solving the spherical Nilsson Hamiltonian, the efficiency and the numerical accuracy of these treatments will be demonstrated in Sec. IV D.

A. The l^2 divergence problem

The l^2 divergence problem resulting from the $D[l^2 - \langle l^2 \rangle_N]$ term in Eq. (1) will occur in high- l case. In the following, the divergence problem will be shown explicitly with spherical Nilsson Hamiltonian. In spherical case, the eigen state of the Nilsson Hamiltonian is $|Nlj\Omega\rangle$, and the contribution of $D[l^2 - \langle l^2 \rangle_N]$ term to the single-particle energy can be calculated as

$$\begin{aligned} & D[l^2 - \langle l^2 \rangle_N] |Nlj\Omega\rangle \\ &= \frac{1}{2} D [l^2 - (4n_r + 1)l - 6n_r] |Nlj\Omega\rangle, \quad N = 2n_r + 1 \end{aligned} \quad (13)$$

where n_r is the radial node number. Considering that $D < 0$ in general case, the single-particle energy will approach negative infinity as $l \rightarrow \infty$.

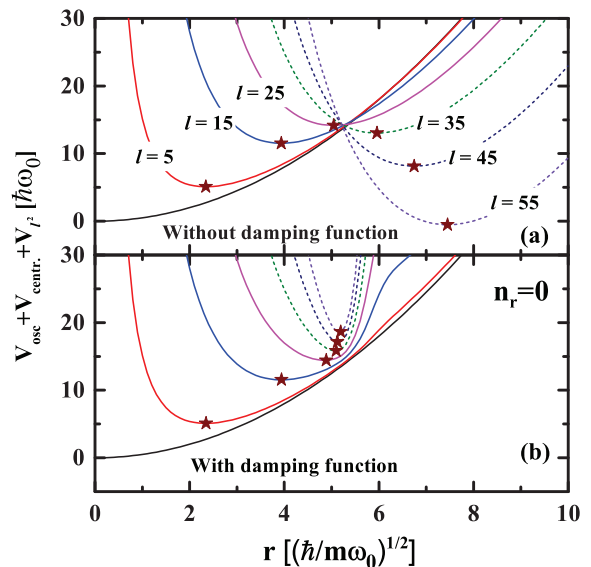


FIG. 1: (Color online) (a) Effective radial potential, $V_{\text{eff.}}(r) = V_{\text{osc.}}(r) + V_{\text{centr.}}(r) + V_{l^2}(r)$, of the spherical Nilsson Hamiltonian for a given orbital quantum number l , when the radial number $n_r = 0$; (b) Same as panel (a), but the term $V_{l^2}(r)$ therein has been modified by the damping function $f_D(r)$ in Eq. (15). The minimum of the effective potential for a given orbital quantum number is labeled as pentagram.

To have a closer look, we define the effective radial potential,

$$\begin{aligned} V_{\text{eff.}}(r) &= V_{\text{osc.}}(r) + V_{\text{centr.}}(r) + V_{l^2}(r) \\ &= \frac{1}{2}r^2 + \frac{l(l+1)}{2r^2} + \frac{1}{2}D [l^2 - (4n_r + 1)l - 6n_r], \end{aligned} \quad (14)$$

where the centrifugal potential $V_{\text{centr.}}(r)$ and the $D[\mathbf{l}^2 - \langle \mathbf{l}^2 \rangle_N]$ term $V_{\mathbf{l}^2}(r)$ are included. Taking radial node number $n_r = 0$ as an example, we show $V_{\text{eff.}}(r)$ for various l -values in Fig. 1(a). From Fig. 1(a), the minimum of $V_{\text{eff.}}(r)$ goes upward with the increase of l when $l < 25$. However, in the high- l cases ($l > 25$), the minimum goes downward and even become negative. Obviously, these high- l states are non-physical solutions, and should not be considered. In H.O. basis calculation, these high- l states are excluded automatically due to the truncation of model space. In 3D lattice space, however, it takes into account equivalently a large H.O. basis, so that these high- l states will be included and leads to the divergence problem of the 3D lattice calculation.

From Fig. 1(a), it can be found that radial position of the minimum of $V_{\text{eff.}}(r)$ increases monotonically with l . Therefore, we propose to restrict the action region of $D\mathbf{l}^2$ to a moderate space. In order to realise the restriction of the action region of $D\mathbf{l}^2$, the Fermi-type damping function is introduced,

$$f_D(r) = \frac{1}{1 + e^{(r-r_D)/a_D}}, \quad (15)$$

where the parameter r_D is an effective cut-off and a_D is smooth parameter. Then, $D\mathbf{l}^2$ is divided into two parts, i.e., $Df_D(r)\mathbf{l}^2 f_D(r)$ and $D[\mathbf{l}^2 - f_D(r)\mathbf{l}^2 f_D(r)]$, and the second part will be regarded as perturbation in the calculations.

There are two considerations for the choosing of damping parameters r_D and a_D . One is that the $V_{\text{eff.}}(r)$ of unphysical high- l states should be raised properly, and another is that the effects for the $V_{\text{eff.}}(r)$ of physical low- l states should be small. In present work, $r_D = 6$ and $a_D = 0.2$ are adopted, and the corresponding effective radial potentials are shown in Fig. 1(b) from which one can find that these two criterions are fulfilled quite well. The effects of the damping function for the single-particle states $|\psi\rangle$ could be evaluated quantitatively by the first order correction $\Delta E_{\text{damping}}^{(1)} = \langle \psi | \mathbf{l}^2 - f_D(r)\mathbf{l}^2 f_D(r) | \psi \rangle$, and the detailed discussion in spherical case can be found in Sec. IV D.

B. The calculation of the $\langle \mathbf{l}^2 \rangle_N$ term

The calculation of $\langle \mathbf{l}^2 \rangle_N$ term is trivial in spherical harmonic basis representation as N is a good quantum number. However, the calculation of the $\langle \mathbf{l}^2 \rangle_N$ term in 3D lattice space is troublesome as there is no quantum number N . To calculate this term in 3D lattice space, we will rewrite $\langle \mathbf{l}^2 \rangle_N$ as a N -independent operator form.

In spherical harmonic basis representation, $\langle \mathbf{l}^2 \rangle_N$ and $\hat{h}_0 = -(\Delta + r^2)/2$ contribute only to the diagonal element with $N(N+3)/2$ and $N+3/2$ respectively, so $\langle \mathbf{l}^2 \rangle_N$ can be replaced as,

$$\langle \mathbf{l}^2 \rangle_N = \frac{N(N+3)}{2}$$

$$= \langle Nlj\Omega | (\hat{h}_0 - 3/2) (\hat{h}_0 + 3/2) | Nlj\Omega \rangle. \quad (16)$$

Due to the orthogonal completeness of the basis, $\langle \mathbf{l}^2 \rangle_N \equiv \hat{h}_0^2 - 9/2$, and by replacing the $\langle \mathbf{l}^2 \rangle_N$ term in Hamiltonian with $\hat{h}_0^2 - 9/2$ one can calculate it in the 3D lattice space.

C. The improvement of the convergence in the 3D lattice calculation

Another practical problem is that the potential $V(r, \theta)$ used in Nilsson Hamiltonian (1) increases as r^2 with $r \rightarrow \infty$, which appreciably contributes to the states $\{\phi_k\}$ in Eq. (11) with high energy, and makes the iteration in Eq. (12) converging slowly and even running into pathological result. In Sec. IV B, the potential $V_0(r) = r^2/2$ introduced in $\hat{h}_0^2 - 9/2$ also leads the similar problem. In order to improve the convergence of the iteration, the potential $V(r, \theta)$ and $V_0(r)$ can be modified as $V(r, \theta) = \min\{V(r, \theta), V_{\text{cut1}}\}$ and $V_0(r) = \min\{V_0(r), V_{\text{cut2}}\}$, respectively. In the practical calculation, we find that $V_{\text{cut1}} = 40 [\hbar\omega_0]$ and $V_{\text{cut2}} = 16 [\hbar\omega_0]$ give a good convergence feature. Considering that the energies of the interesting levels are under 7 $[\hbar\omega_0]$, the values of $V_{\text{cut1}} = 40 [\hbar\omega_0]$ and $V_{\text{cut2}} = 16 [\hbar\omega_0]$ are reasonable for the description of these levels.

D. Numerical accuracy of the 3D lattice calculation

In order to examine the efficiency of the numerical techniques introduced in above, 3D lattice calculation is used to solve the spherical Nilsson Hamiltonian, and with taking first order perturbation correction of damping function, the accuracy of the calculation is checked by comparing the obtained single-particle energies with exact solutions.

As shown in Fig. 2(a), the absolute deviations of single-particle energies between the 3D lattice calculations and the exact solutions are given as a function of single-particle energy for $a_D = 0.1$ and 0.2 case, respectively. Meanwhile, the corresponding first order correction $\Delta E_{\text{damping}}^{(1)}$ are shown in Fig. 2(b).

It can be seen that the absolute deviations between the 3D lattice calculations and the exact solutions are smaller than $10^{-5}[\hbar\omega_0]$ for $a_D = 0.1$ and 0.2 case, which indicate the high accuracy of the present calculation with the numerical techniques introduced in Sec. IV. From Fig. 2(b), the first order corrections $\Delta E_{\text{damping}}^{(1)}$ are smaller than $10^{-5}[\hbar\omega_0]$ and $10^{-7}[\hbar\omega_0]$, and they are much less than single-particle energies, so regarding $D[\mathbf{l}^2 - f_D(r)\mathbf{l}^2 f_D(r)]$ as a perturbation term is reasonable. Comparing Fig. 2(a) and 2(b), one can find that the decrease of $\Delta E_{\text{damping}}^{(1)}$ are almost two orders of magnitude from $a_D = 0.2$ to 0.1, while the accuracy of the 3D lattice calculation remains nearly unchanged. So one can

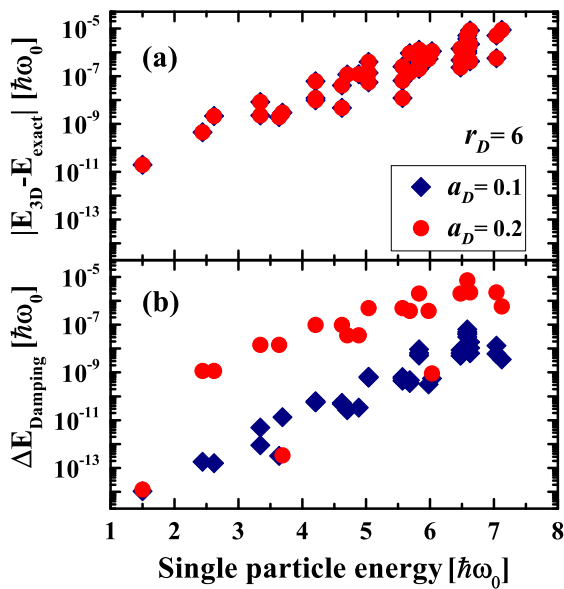


FIG. 2: (Color online) For a spherical Nilsson Hamiltonian, the absolute deviations of single-particle energies obtained by the 3D lattice calculation from the exact results (a) and the first-order corrections to the single-particle energies introduced by the damping function (b) as functions of the single particle energy. The red dots and the blue lozenges represent the results with the damping factor $a_D=0.1$ and 0.2 , respectively.

conclude that the deviations in Fig. 2(a) do not originate from the introducing damping function.

V. SINGLE PARTICLE IN A REFLECTION-ASYMMETRIC POTENTIAL

In this section, the single-particle motion in a reflection-asymmetric deformed potential is solved by ITM in 3D lattice space with the numerical techniques mentioned in Sec. IV. As comparisons, the corresponding Schrödinger equation of the Hamiltonian is also diagonalized by using the spherical Harmonic oscillator basis.

In Fig. 3, we show the single-particle levels as functions of quadrupole deformation β_2 on the left panel and octupole deformation β_3 with β_2 fixed on the right panel. The lines with various colors represent the results obtained by H.O. basis calculation, and the red (blue) lines denote the levels with positive (negative) parity. The dots represent the results obtained by 3D lattice calculation. It can be seen that the agreement between 3D lattice calculation and H.O. basis calculation is very satisfactory. For the single-particle levels shown in Fig. 3, all the differences between these two numerical methods are smaller than $10^{-4} [\hbar\omega_0]$, which demonstrate the high accuracy and good reliability of these two numerical methods.

For the reflection-symmetric case ($\beta_3 = 0$) as shown in Fig. 3(a), it can be found that the calculations give

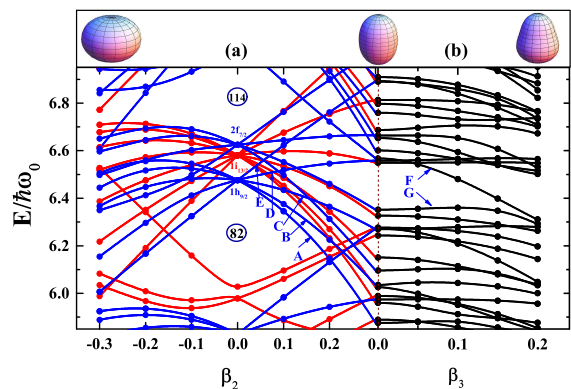


FIG. 3: (Color online) The single-particle levels, obtained by the 3D lattice calculation (dots) and the H.O. basis calculation (lines), as functions of the deformation parameters β_2 and β_3 . The red (blue) represents positive (negative) parity. The shapes shown in the top panel correspond to the deformation parameters $(\beta_2, \beta_3) = (-0.3, 0), (0.3, 0), (0.3, 0.2)$, respectively.

a sizeable energy gap at proton numbers 82 and 114 in spherical case, which reproduce the traditional proton magic number 82 and suggest the proton magic number 114 for superheavy nuclei. There are three spherical orbits, i.e., $1h_{9/2}$, $1i_{13/2}$, $2f_{7/2}$, between these two gaps. With the quadrupole deformation β_2 introduced, the degeneracy due to spherical symmetry is removed, and the energy gaps at 82 and 114 are quenched. In order to investigate the evolution of the deformed single-particle levels, the levels coming from $1h_{9/2}$ are chosen, where the Level A~E denote the levels with z -components of total angular momenta $\Omega = 1/2 \sim 9/2$. It can be found that, for $\beta_2 > 0$ (prolate shape), the energy Levels A~E drop rapidly with β_2 for low Ω values increases sharply with Ω . For $\beta_2 < 0$ (oblate shape), the opposite feature of this levels are shown in the small deformation region, while Levels A~E all show a decrease trend in a larger deformation region. The slope of the energy Level A~E could be evaluated by the first order perturbation correction of the quadrupole operator $q = r^2 Y_{20}$ [2].

For the reflection-asymmetric case ($\beta_3 \neq 0$) as shown in Fig. 3(b), the evolution of most energy levels with respect to β_3 is rather slowly. Due to the odd parity of operator $r^2 Y_{30}$, its first order perturbation correction vanishes, therefore, the slope of the energy levels with respect to β_3 may be evaluated by the second order perturbation correction, which gives rather gentle slope compared to quadruple deformed case. However, some levels show more drastic change with increase of β_3 , and it can be understood by analysing the octupole coupling of the energy levels. It is well known that the condition for strong octupole coupling is driven by the interaction between the orbitals (l, j) and $(l \pm 3, j \pm 3)$ through the Y_{30} potential [61]. In order to understand the evolution of energy levels with the deformation β_3 , the Level F and G coming from $2f_{5/2}$ and $2f_{7/2}$ are chosen. These levels together

TABLE I: Single-particle levels F and G together with the corresponding contributions from the five leading components for $(\beta_2, \beta_3) = (0.3, 0), (0.3, 0.1), (0.3, 0.2)$, respectively.

(β_2, β_3)	Level	1st comp.	2nd comp.	3rd comp.	4th comp.	5th comp.
(0.3,0.0)	F	$[5, 3, \frac{5}{2}, \frac{1}{2}]$ 30.7%	$[5, 1, \frac{1}{2}, \frac{1}{2}]$ 20.9%	$[5, 3, \frac{7}{2}, \frac{1}{2}]$ 17.2%	$[5, 5, \frac{9}{2}, \frac{1}{2}]$ 13.6%	$[7, 7, \frac{15}{2}, \frac{1}{2}]$ 6.4%
	G	$[5, 3, \frac{7}{2}, \frac{3}{2}]$ 65.2%	$[5, 5, \frac{9}{2}, \frac{3}{2}]$ 9.4%	$[5, 1, \frac{3}{2}, \frac{3}{2}]$ 9.4%	$[5, 5, \frac{11}{2}, \frac{3}{2}]$ 6.1%	$[7, 5, \frac{11}{2}, \frac{3}{2}]$ 2.7%
(0.3,0.1)	F	$[7, 7, \frac{15}{2}, \frac{1}{2}]$ 18.0%	$[5, 3, \frac{7}{2}, \frac{1}{2}]$ 13.4%	$[5, 5, \frac{9}{2}, \frac{1}{2}]$ 11.3%	$[5, 3, \frac{5}{2}, \frac{1}{2}]$ 8.8%	$[6, 6, \frac{13}{2}, \frac{1}{2}]$ 8.4%
	G	$[5, 3, \frac{7}{2}, \frac{3}{2}]$ 60.1%	$[5, 1, \frac{3}{2}, \frac{3}{2}]$ 9.0%	$[5, 5, \frac{9}{2}, \frac{3}{2}]$ 7.7%	$[7, 7, \frac{15}{2}, \frac{3}{2}]$ 5.1%	$[5, 5, \frac{11}{2}, \frac{3}{2}]$ 2.9%
(0.3,0.2)	F	$[6, 6, \frac{13}{2}, \frac{1}{2}]$ 33.2%	$[5, 5, \frac{9}{2}, \frac{1}{2}]$ 13.1%	$[7, 7, \frac{15}{2}, \frac{1}{2}]$ 9.4%	$[5, 3, \frac{7}{2}, \frac{1}{2}]$ 6.3%	$[4, 2, \frac{5}{2}, \frac{1}{2}]$ 2.7%
	G	$[5, 3, \frac{7}{2}, \frac{3}{2}]$ 38.9%	$[7, 7, \frac{15}{2}, \frac{3}{2}]$ 12.9%	$[6, 6, \frac{13}{2}, \frac{3}{2}]$ 5.9%	$[5, 5, \frac{9}{2}, \frac{3}{2}]$ 5.7%	$[5, 5, \frac{3}{2}, \frac{3}{2}]$ 4.8%

with their contributions from the five leading components (labeled by the spherical quantum numbers $[Nlj\Omega]$) for the $(\beta_2, \beta_3) = (0.3, 0), (0.3, 0.1), (0.3, 0.2)$ cases are shown in Table I, respectively. For the Level F with a drastically decreasing tendency, its second (13.4%) and third (8.4%) components compose an octupole deformation driving pairs $2f_{7/2}[5, 3, \frac{7}{2}, \frac{1}{2}]$ and $i_{13/2}[6, 6, \frac{13}{2}, \frac{1}{2}]$ in the $(\beta_2, \beta_3) = (0.3, 0.1)$ case. The weight of this driving pair grows with the increase of β_3 , and a successive decrease in energy level F is given. For the Level G with a slowly decreasing tendency, no octupole deformation driving pairs are found among the five leading components in the $(\beta_2, \beta_3) = (0.3, 0.1)$ case. With the increase of β_3 , the octupole deformation driving pair $f_{7/2}[5, 3, \frac{7}{2}, \frac{1}{2}]$ and $i_{13/2}[6, 6, \frac{13}{2}, \frac{1}{2}]$ composed by the first (38.9%) and second (5.9%) components appears, and the energy level G shows an obvious decreasing tendency. Therefore, the tendency of energy levels with the octupole deformation can be well understood by the octupole coupling between the octupole deformation driving pairs.

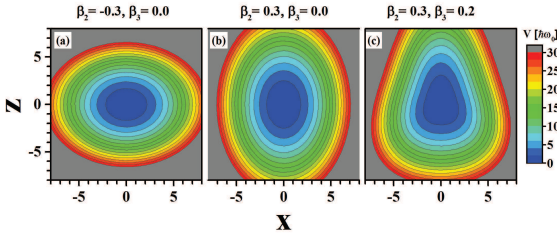


FIG. 4: (Color online) Contour plots of the reflection-asymmetric Nilsson potentials on the plane determined by the x-axis and the axially symmetric z-axis. The deformation parameters corresponding to (a), (b) and (c) are $(\beta_2, \beta_3) = (-0.3, 0), (0.3, 0), (0.3, 0.2)$, respectively.

Furthermore, all these evolution features can be also understood by comparing the shapes of potential and the density distribution of single particle levels. In order to better understand the behaviors of the single-particle levels in a given reflection-asymmetric deformed potential, Fig. 4 displays the distribution of the reflection-asymmetric deformed potential with $(\beta_2, \beta_3) = (-0.3, 0), (0.3, 0), (0.3, 0.2)$ in $y = 0$ plane, and the corresponding single particle densities of Level A~E in the xz plane at the positions of grid point in y directions closest to zero,

namely, at $y = d/2 = 0.3$ are depicted in Fig.5.

The quadrupole field r^2Y_{20} causes the levels with lower Ω values to be shifted downwards for positive deformations (prolate shapes) and to be shifted upwards for negative deformation (oblate shapes). One can understand this effect, realizing that the states with lower Ω -values have a relatively higher probability of being close to z -axis. Comparing Fig. 4(a) and 4(b), it can be found that the potential gets softer in z -direction and steeper in xy -directions with the increase of β_2 . The single particle density distributions for Levels A~E in $(\beta_2, \beta_3) = (0.3, 0)$ case are shown in the second row of Fig. 5. The density distribution of Level A is mainly near z -axis, and a softer potential in z -direction will move down the energy of this level. Similarly, the density distribution of Level E is mainly near $z = 0$ plane, and a steeper potential in xy -direction will move up the energy of this level. According to the above discussion, the evolution of Levels A~E with respect to β_2 shown in Fig. 3(a) could be understood properly. For the $(\beta_2, \beta_3) = (-0.3, 0)$ case, all the single particle density distributions of level A~E have considerable parts distribute closely to $z = 0$ plane as shown in the first row of Fig. 5, therefore, level A~E go downwards with decrease of β_2 in the large oblate deformed region.

Comparing Fig. 4(b) and 4(c), the potential changes rather slightly, and it is nearly unchanged in z -direction and gets steeper (softer) in xy -directions for $z > 0$ ($z < 0$) with the increase of β_3 . The density distributions of level A~E in $(\beta_2, \beta_3) = (0.3, 0.2)$ case are shown in the third row of Fig. 5, and compared with the second row of Fig. 5, one should note that the change of density distributions is not so drastic, which is consistent with the slow evolution with increase of β_3 . One can also find the single particle density distribution of the levels with lower Ω show pronounced reflection-asymmetric structure, therefore, the occupation of these levels likely leads to a reflection-asymmetric shape.

VI. SUMMARY AND PERSPECTIVES

In summary, the imaginary time method in 3D lattice space and the harmonic oscillator basis expansion method has been applied to investigate the single-particle

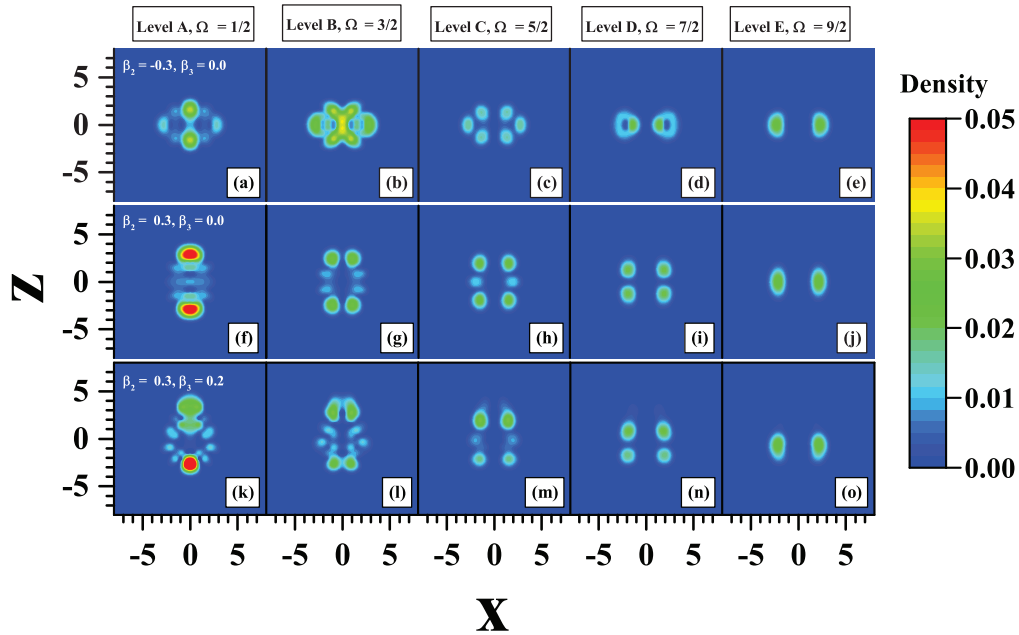


FIG. 5: (Color online) The density distributions versus x and z on the $y = 0.3$ plane for the levels A-E shown in Fig. 3 obtained by the 3D lattice calculations. The deformation parameters are $(\beta_2, \beta_3) = (-0.3, 0), (0.3, 0), (0.3, 0.2)$, respectively.

motion in a reflection-asymmetric potential by solving the reflection-asymmetric Nilsson Hamiltonian. Several numerical challenges occur when the Nilsson Hamiltonian is solved in 3D lattice space, and have been discussed and overcome with special numerical techniques: (i) the l^2 divergence problem is solved by introducing the damping function; (ii) the challenge of calculating $\langle l^2 \rangle_N$ term due to the missing of quantum number N is overcome by replacing $\langle l^2 \rangle_N$ with an equivalent N -independent operator form; (iii) the convergence problem owing to the potential used in Nilsson Hamiltonian increases dramatically as $r \rightarrow \infty$ is improved by modifying the potential. The efficiency of these special numerical techniques is demonstrated by solving the spherical Nilsson Hamiltonian in 3D lattice space. Then, the single-particle motion in a reflection-asymmetric deformed potential is solved by the above two numerical methods. The consistency of these two methods is demonstrated by that the differences in the obtained single-particle energy are smaller than $10^{-4}[\hbar\omega_0]$. The tendency of the energy levels with the quadrupole and octupole deformation can be well understood by the first order perturbation correction of the quadrupole operator $q = r^2 Y_{20}$ and the octupole coupling between the octupole deformation driving pairs, respectively. The evolution of the deformed single-particle levels is also understood by comparing the single-particle density distribution and the distribution of the reflection-

asymmetric deformed potential.

Based on the present work for solving the single-particle motion in a reflection-asymmetric Nilsson potential, the reflection-asymmetric particle rotor model is expected to be developed. There are several works that have been done to explain the spectroscopic properties of axial reflection-asymmetric nuclei using concepts based on the particle rotor model [62, 63]. Similar to those works, with further including the triaxial deformation degree of freedom, we can develop the triaxial reflection-asymmetric particle rotor model, which is expected to achieve the interpretation of the observed multiple chiral doublet bands with octupole correlations in ^{78}Br recently [64].

Acknowledgments

The authors are indebted to Prof. Jie Meng for constructive guidance and valuable suggestions. Fruitful discussions with Prof. Shuangquan Zhang are highly acknowledged. This work was supported in part by the Major State 973 Program of China (Grant No. 2013CB834400), the National Natural Science Foundation of China (Grants No. 11335002, No. 11375015, No. 11461141002, and No. 11621131001).

[1] A. Bohr and B. R. Mottelson, *Nuclear structure, vol. ii* (1975).

[2] P. Ring and P. Schuck, *The nuclear many-body problem* (Springer Science & Business Media, 2004).

- [3] I. Tanihata, H. Hamagaki, O. Hashimoto, Y. Shida, N. Yoshikawa, K. Sugimoto, O. Yamakawa, T. Kobayashi, and N. Takahashi, Phys. Rev. Lett. **55**, 2676 (1985), URL <https://link.aps.org/doi/10.1103/PhysRevLett.55.2676>.
- [4] J. Meng and P. Ring, Phys. Rev. Lett. **77**, 3963 (1996), URL <https://link.aps.org/doi/10.1103/PhysRevLett.77.3963>.
- [5] J. Meng and P. Ring, Phys. Rev. Lett. **80**, 460 (1998), URL <https://link.aps.org/doi/10.1103/PhysRevLett.80.460>.
- [6] J. Meng, H. Toki, S.-G. Zhou, S. Q. Zhang, W. H. Long, and L. S. Geng, Prog. Part. Nucl. Phys. **57**, 470 (2006), ISSN 0146-6410, URL <http://www.sciencedirect.com/science/article/pii/S014664100500075X>.
- [7] S.-G. Zhou, J. Meng, P. Ring, and E.-G. Zhao, Phys. Rev. C **82**, 011301 (2010), URL <https://link.aps.org/doi/10.1103/PhysRevC.82.011301>.
- [8] J. Meng and S.-G. Zhou, J. Phys. G: Nucl. Part. Phys. **42**, 093101 (2015), URL <http://stacks.iop.org/0954-3899/42/i=9/a=093101>.
- [9] P. J. Twin, B. M. Nyakó, A. H. Nelson, J. Simpson, M. A. Bentley, H. W. Cranmer-Gordon, P. D. Forsyth, D. Howe, A. R. Mokhtar, J. D. Morrison, et al., Phys. Rev. Lett. **57**, 811 (1986), URL <https://link.aps.org/doi/10.1103/PhysRevLett.57.811>.
- [10] S. Frauendorf, Y. Gu, and J. Sun, Int. J. Mod. Phys. E **20**, 465 (2011).
- [11] Y. Y. Wang, Z. Shi, Q. B. Chen, S. Q. Zhang, and C. Y. Song, Phys. Rev. C **93**, 044309 (2016), URL <https://link.aps.org/doi/10.1103/PhysRevC.93.044309>.
- [12] S. Frauendorf and J. Meng, Nucl. Phys. A **617**, 131 (1997), URL <http://www.sciencedirect.com/science/article/pii/S0375947497000043>.
- [13] S. Frauendorf, Rev. Mod. Phys. **73**, 463 (2001), URL <https://link.aps.org/doi/10.1103/RevModPhys.73.463>.
- [14] J. Meng and S. Q. Zhang, J. Phys. G: Nucl. Part. Phys. **37**, 064025 (2010), URL <http://stacks.iop.org/0954-3899/37/i=6/a=064025>.
- [15] S. W. Ødegård, G. B. Hagemann, D. R. Jensen, M. Bergström, B. Herskind, G. Sletten, S. Törmänen, J. N. Wilson, P. O. Tjøm, I. Hamamoto, et al., Phys. Rev. Lett. **86**, 5866 (2001), URL <https://link.aps.org/doi/10.1103/PhysRevLett.86.5866>.
- [16] M. G. Mayer, Phys. Rev. **75**, 1969 (1949), URL <https://link.aps.org/doi/10.1103/PhysRev.75.1969>.
- [17] J. Rainwater, Phys. Rev. **79**, 432 (1950), URL <https://link.aps.org/doi/10.1103/PhysRev.79.432>.
- [18] A. Bohr, Dan. Vidensk. Selsk **26**, 1 (1952).
- [19] S. G. Nilsson, S. Nilsson, et al., Mat. Fys. Medd. Dan. Vid. Selsk **29**, 1 (1955).
- [20] F. S. Stephens, F. Asaro, and I. Perlman, Phys. Rev. **100**, 1543 (1955), URL <https://link.aps.org/doi/10.1103/PhysRev.100.1543>.
- [21] V. Strutinsky, Atomnaya energiya **4**, 150 (1956).
- [22] K. Lee and D. R. Inglis, Phys. Rev. **108**, 774 (1957), URL <https://link.aps.org/doi/10.1103/PhysRev.108.774>.
- [23] I. Dutt and P. Mukherjee, Prog. Theor. Phys **22**, 814 (1959), URL <http://dx.doi.org/10.1143/PTP.22.814>.
- [24] M. Rustgi and S. Mukherjee, Phys. Rev. **131**, 2615 (1963).
- [25] P. Vogel, Phys. Lett. B **25**, 65 (1967).
- [26] P. Moller, S. Nilsson, A. Sobczewski, Z. Szymanski, and S. Wycech, Phys. Lett. B **30**, 223 (1969), ISSN 0370-2693, URL <https://www.sciencedirect.com/science/article/pii/0370269369904225>.
- [27] G. Leander and S. Larsson, Nucl. Phys. A **239**, 93 (1975), ISSN 0375-9474, URL <http://www.sciencedirect.com/science/article/pii/0375947475911367>.
- [28] J. Meng, K. Sugawara-Tanabe, S. Yamaji, and A. Arima, Phys. Rev. C **59**, 154 (1999), URL <https://link.aps.org/doi/10.1103/PhysRevC.59.154>.
- [29] T. S. Chen, H. F. Lu, J. Meng, S. Q. Zhang, and S.-G. Zhou, Chin. Phys. Lett. **20**, 358 (2003), URL http://cpl.iphy.ac.cn/EN/abstract/article_36854.shtml.
- [30] S.-G. Zhou, J. Meng, and P. Ring, Phys. Rev. Lett. **91**, 262501 (2003), URL <https://link.aps.org/doi/10.1103/PhysRevLett.91.262501>.
- [31] H. Z. Liang, J. Meng, and S.-G. Zhou, Phys. Rep. **570**, 1 (2015), ISSN 0370-1573, hidden pseudospin and spin symmetries and their origins in atomic nuclei, URL <https://www.sciencedirect.com/science/article/pii/S0370157315000502>.
- [32] J. Meng, ed., *Relativistic Density Functional for Nuclear Structure*, vol. 10 of *International Review of Nuclear Physics* (World Scientific, Singapore, 2016).
- [33] A. V. Afanasjev, D. B. Fossan, G. J. Lane, and I. Ragnarsson, Phys. Rep. **322**, 1 (1999), ISSN 0370-1573, URL <https://www.sciencedirect.com/science/article/pii/S0370157399000356>.
- [34] D. Vretenar, A. V. Afanasjev, G. A. Lalazissis, and P. Ring, Phys. Rep. **409**, 101 (2005), ISSN 0370-1573, URL <https://www.sciencedirect.com/science/article/pii/S0370157304004545>.
- [35] T. Nikšić, Z. P. Li, D. Vretenar, L. Próchniak, J. Meng, and P. Ring, Phys. Rev. C **79**, 034303 (2009), URL <https://link.aps.org/doi/10.1103/PhysRevC.79.034303>.
- [36] Z. P. Li, T. Nikšić, D. Vretenar, J. Meng, G. A. Lalazissis, and P. Ring, Phys. Rev. C **79**, 054301 (2009), URL <https://link.aps.org/doi/10.1103/PhysRevC.79.054301>.
- [37] P. W. Zhao, J. Peng, H. Z. Liang, P. Ring, and J. Meng, Phys. Rev. Lett. **107**, 122501 (2011), URL <https://link.aps.org/doi/10.1103/PhysRevLett.107.122501>.
- [38] J. Meng and P. W. Zhao, Phys. Scripta **91**, 053008 (2016), URL <http://stacks.iop.org/1402-4896/91/i=5/a=053008>.
- [39] J. Meng, J. Peng, S. Q. Zhang, and P. W. Zhao, Front. Phys. **8**, 55 (2013).
- [40] J. M. Yao, N. Itagaki, and J. Meng, Phys. Rev. C **90**, 054307 (2014), URL <https://link.aps.org/doi/10.1103/PhysRevC.90.054307>.
- [41] J. M. Yao, E. F. Zhou, and Z. P. Li, Phys. Rev. C **92**, 041304 (2015), URL <https://link.aps.org/doi/10.1103/PhysRevC.92.041304>.
- [42] P. W. Zhao, N. Itagaki, and J. Meng, Phys. Rev. Lett. **115**, 022501 (2015), URL <https://link.aps.org/doi/10.1103/PhysRevLett.115.022501>.
- [43] E. F. Zhou, J. M. Yao, Z. P. Li, J. Meng, and P. Ring, Phys. Lett. B **753**, 227 (2016), ISSN 0370-2693, URL <http://www.sciencedirect.com/science/article/pii/S0370269315009764>.
- [44] M. Bender, P.-H. Heenen, and P.-G. Reinhard, Rev. Mod.

- Phys. **75**, 121 (2003), URL <https://link.aps.org/doi/10.1103/RevModPhys.75.121>.
- [45] L. S. Geng, J. Meng, and H. Toki, Chin. Phys. Lett. **24**, 1865-1868 (2007), URL http://cpl.iphy.ac.cn/EN/abstract/article_36535.shtml.
- [46] J.-Y. Guo, P. Jiao, and X.-Z. Fang, Phys. Rev. C **82**, 047301 (2010), URL <https://link.aps.org/doi/10.1103/PhysRevC.82.047301>.
- [47] W. Zhang, Z. P. Li, and S. Q. Zhang, Chin. Phys. C **34**, 1094 (2010), URL <http://stacks.iop.org/1674-1137/34/i=8/a=011>.
- [48] B.-N. Lu, E.-G. Zhao, and S.-G. Zhou, Phys. Rev. C **85**, 011301 (2012), URL <https://link.aps.org/doi/10.1103/PhysRevC.85.011301>.
- [49] J. Zhao, B.-N. Lu, T. Nikšić, and D. Vretenar, Phys. Rev. C **92**, 064315 (2015), URL <https://link.aps.org/doi/10.1103/PhysRevC.92.064315>.
- [50] J. Zhao, B.-N. Lu, T. Nikšić, D. Vretenar, and S.-G. Zhou, Phys. Rev. C **93**, 044315 (2016), URL <https://link.aps.org/doi/10.1103/PhysRevC.93.044315>.
- [51] S.-G. Zhou, Phys. Scripta **91**, 063008 (2016), URL <http://stacks.iop.org/1402-4896/91/i=6/a=063008>.
- [52] K. Davies, H. Flocard, S. Krieger, and M. Weiss, Nucl. Phys. A **342**, 111 (1980), ISSN 0375-9474, URL <http://www.sciencedirect.com/science/article/pii/0375947480905096>.
- [53] K. Hagino and Y. Tanimura, Phys. Rev. C **82**, 057301 (2010).
- [54] J. Maruhn, P.-G. Reinhard, P. Stevenson, and A. Umar, Computer Physics Communications **185**, 2195 (2014).
- [55] Y. Tanimura, K. Hagino, and H. Z. Liang, Prog. Theor. Exp. Phys. **2015**, 073D01 (2015).
- [56] Z. X. Ren, S. Q. Zhang, and J. Meng, Phys. Rev. C **95**, 024313 (2017), URL <https://link.aps.org/doi/10.1103/PhysRevC.95.024313>.
- [57] S. G. Nilsson and I. Ragnarsson, *Shapes and shells in nuclear structure* (Cambridge Cambridge University Press, 1995), includes bibliographical references (p. 399-404) and index, URL <http://openlibrary.org/books/OL1100790M>.
- [58] S. G. Nilsson, C. F. Tsang, A. Sobczewski, Z. Szymański, S. Wycech, C. Gustafson, I.-L. Lamm, P. Möller, and B. Nilsson, Nucl. Phys. A **131**, 1 (1969), ISSN 0375-9474, URL <http://www.sciencedirect.com/science/article/pii/0375947469908094>.
- [59] P.-G. Reinhard and R. Cusson, Nucl. Phys. A **378**, 418 (1982).
- [60] V. Blum, G. Lauritsch, J. Maruhn, and P.-G. Reinhard, Journal of Computational Physics **100**, 364 (1992), ISSN 0021-9991, URL <http://www.sciencedirect.com/science/article/pii/002199919290242Q>.
- [61] A. N. Bohr and B. R. Mottelson, Dan. Mat. Fys. Medd. **27**, 1 (1953).
- [62] D. Zaikin, Nucl. Phys. **86**, 638 (1966), ISSN 0029-5582, URL <http://www.sciencedirect.com/science/article/pii/0029558266905025>.
- [63] G. Leander and R. Sheline, Nucl. Phys. A **413**, 375 (1984), ISSN 0375-9474, URL <http://www.sciencedirect.com/science/article/pii/0375947484904172>.
- [64] C. Liu, S. Y. Wang, R. A. Bark, S. Q. Zhang, J. Meng, B. Qi, P. Jones, S. M. Wyngaardt, J. Zhao, C. Xu, et al., Phys. Rev. Lett. **116**, 112501 (2016), URL <https://link.aps.org/doi/10.1103/PhysRevLett.116.112501>.